Phys. Status Solidi A **208**, No. 9, 2099–2103 (2011) / **DOI** 10.1002/pssa.201100036

physica status solidi a
www.pss-a.com
applications and materials science

# Monitoring of peptide induced disruption of artificial lipid membrane constructed on boron-doped nanocrystalline diamond by electrochemical impedance spectroscopy

**Václav Petrák*[,1], Lars Grieten[2], Andrew Taylor[3], František Fendrych[3], Miroslav Ledvina[4], Stoffel D. Janssens[2], Miloš Nesládek[2,5], Ken Haenen[2,5], and Patrick Wagner[2,5]**

[1] Faculty of Biomedical Engineering, Czech Technical University in Prague, Sítná sq. 3105, 272 01 Kladno, Czech Republic
[2] Institute for Materials Research (IMO), Hasselt University, Wetenschapspark 1, 3590 Diepenbeek, Belgium
[3] Institute of Physics, Academy of Sciences of the Czech Republic, v.v.i, Prague 8, Czech Republic
[4] Institute of Organic Chemistry and Biochemistry, Academy of Sciences of the Czech Republic, v.v.i., Flemingovo No. 2, 166 10 Prague 6, Czech Republic
[5] IMOMEC Division, IMEC, Institute for Materials Research, University Hasselt, Wetenschapspark 1, 3590 Diepenbeek, Belgium

Received 20 March 2011, revised 3 August 2011, accepted 4 August 2011
Published online 26 August 2011

**Keywords** biosensor, boron-doped nanocrystalline diamond, electrochemical impedance spectroscopy

* Corresponding author: e-mail vaclav.petrak@fbmi.cvut.cz, Phone: +420 266 052 634, Fax: +420 312 608 204

With the rise of antibiotic resistance of pathogenic bacteria there is an increased demand for monitoring of the functionality of bacteria membranes, whose disruption can be induced by peptide–lipid interactions. In this work we attempt to monitor formation and subsequent peptide induced disruption of supported lipid membranes (SLBs) on boron-doped nanocrystalline diamond (B-NCD). Electrochemical Impedance Spectroscopy (EIS) was used to study *in situ* changes related to lipid membrane formation and disruption by peptide-induced interactions. The observed impedance changes were minimal for oxidized B-NCD samples. The sensitivity for the detection of membrane formation and disruption was significantly higher for hydrogenated B-NCD surfaces. Data modelling indicates large differences in the structure of electrical double layer at the B-NCD/SLB interface for hydrogen and oxygen terminated B-NCD surfaces. For oxidized B-NCD surfaces, EIS changes are negligible.



**1 Introduction** The increase in antibiotic resistance of pathogenic bacteria strains spurs development of novel antibiotics. One promising solution to this problem is the group of antibiotics based on antimicrobial peptides which are an abundant and diverse group of molecules that are produced by many tissues and cell types in a variety of plant and animal species [1]. Their amino acid composition, amphipathicity, cationic charge and size allow them to attach to membrane bilayers and disrupt the membrane by formation of pores [2].

Antimicrobial peptides do not target specific molecular receptors on the microbial surface, but rather interact directly with microbial membranes, which they can rapidly permeabilize [3]. The monitoring of specific peptide–lipid interactions in antibiotic peptides, which affect the functionality of bacterial membranes, can play an important role in the research of new antibiotics [4].

Supported lipid bilayers (SLBs) are commonly investigated as a model system of biological membranes. They are composed of a lipid bilayer adsorbed on the surface of a solid substrate [5]. These structures have been extensively used to study the structure and properties of native biological membranes and biological processes such as molecular recognition, enzymatic catalysis, membrane fusion and cell adhesion [6]. On the other hand, several applications based on lipid membranes have been developed, including biosensors [7]. SLBs can be formed on the oxidized (O-terminated) hydrophilic surface as well as the hydrogenated (H-terminated) hydrophobic surface [8]. Diamond exhibits several special properties, such as good biocompatibility and

a large electrochemical potential window that make it particularly suitable for biosensing [9]. In this application, a boron-doped nanocrystalline diamond (B-NCD) film serves as a solid support for SLBs and an active electrode for electrochemical impedance spectroscopy (EIS) measurement of melittin-induced membrane disruption.

EIS was successfully used for the detection of disruption by melittin on free-standing lipid bilayer [10] as well as on SLBs on gold surfaces [11]. Ang et al. were able to detect membrane disruption of SLBs caused by Magainin II on optically transparent diamond [8]. The EIS detection of membrane disruption by antimicrobial peptide LL-37 was also demonstrated [12].

In this work the focus is given to the effects of surface termination on detection abilities of B-NCD film. We constructed a simple sensor for the detection of disruption of SLBs formed on 200 ppm (*i.e.* below metallic limit) boron-doped NCD electrode that serves as a working electrode. SLBs are disrupted by membrane active peptide melittin. We report results from EIS of membrane disruption on hydrogenated and oxidized surfaces and discuss the influence of B-NCD surface termination on the sensitivity of the sensor.

## 2 Experimental

**2.1 Nanocrystalline diamond synthesis** Planar sensor electrodes were prepared by microwave plasma-enhanced chemical vapour deposition (MW PE-CVD) from methane/hydrogen gas mixtures in an ASTeX reactor as described in Ref. [13]. The substrates were 2 inch silicon wafers (thickness 550 μm, crystalline orientation (100), p-type doped with boron and resistivity from 1 to 20 Ω cm), which were cut into samples of 10 mm by 10 mm after deposition. The diamond layers had a typical thickness of 150 nm with an average grain size of 50 nm as determined by X-ray diffraction and atomic force microscopy. Boron doping of diamond during the CVD deposition was done by adding trimethylboron to the gas mixture with a concentration ratio of 200 ppm B/C. For growth conditions and incorporated B-concentration conditions details see Ref. [14]. The B concentration done by calibration on SIMS data is expected to be $6.5 \times 10^{19}\,\mathrm{cm}^{-3}$, *i.e.* below Mott's metallic limit.

The B-NCD samples served as the working electrode in our home-made set-up that allows impedance read-out. Prior to measurements, the diamond samples were either hydrogenated in $H_2$ plasma (67 hPa, 800 °C, power 4000 W, duration 15 min) or oxidized by UV-ozone for 30 min. The resulting contact wetting-angles were $95° \pm 2°$ for the hydrogenated and $14° \pm 3°$ for the oxidized diamond. Cleaning of the B-NCD samples was done in a mixture of $H_2SO_4/KNO_3$ (2:1 wt%) heated to 250 °C for 10 min. Afterwards the samples were rinsed in DI water and dried under a stream of nitrogen.

**2.2 Liposomes** Phospholipids for membrane formation: 1,2-dioleoyl-sn-glycero-3-phosphocholine (DOPC) and 1,2-dioleoyl-sn-glycero-3-phospho-L-serine (DOPS) in chloroform were purchased from Avanti Polar Lipids (USA). Mellitin was supplied by Sigma Aldrich (USA). The DOPC:DOPS lipids were mixed with a 4:1 ratio. Chloroform was evaporated under a gentle stream of nitrogen. The lipid films were formed on the wall of a glass flask. The film was subsequently placed under a vacuum for 30 min to remove residual solvent. Deionized water was added to redissolve the lipids to give an aqueous suspension of lipids at a concentration of 100 μM. Small unilamellar vesicles, liposomes, were formed by sonicating the lipid suspension for 15 min with UP400S ultrasonic processor (Hielscher, Germany). This method yielded a transparent solution with mean particle size of 75 nm as confirmed by dynamic light scattering.

**2.3 Sensor setup** The B-NCD samples were mounted on a copper backing contact by an electrically conductive eutectic transfer tape. Rubber O-rings (Viton) with an inner diameter of 6 mm were pressed between the active electrode and the body of the sensor forming a cell with a total inner volume of 160 μl. The cell was filled with 140 μl of 10 mM Hepes buffer (4-(2-hydroxyethyl)-1-piperazineethanesulfonic acid) solution with 150 mM NaCl. A gold counter electrode with a 500 μm diameter was immersed in the solution. The working and counter electrodes were connected to the 4194A Impedance/Gain-Phase Analyser (Hewlett Packard, USA) with shielded cables. A schematic cross-section of the setup is shown in Fig. 1.

After stabilization of the system at 25 °C, a 100 μM solution of DOPC:DOPS (4:1) liposomes were added. The membrane is formed by vesicle fusion method. Lipid membrane formation was completed within 30 min. For membrane disruption active amphipathic α-helical peptide, melittin, was added with the concentration of 2 μM.

The impedance was measured by applying an AC potential ($U$) with 10 mV amplitude to the measurement cell. Response to this potential is an AC current signal ($I$). The complex impedance, calculated from the $U/I$ ratio, was measured for 50 frequencies, equidistant on logarithmic scale, in a frequency range from 100 Hz to 1 MHz. The duration of one frequency sweep was 15 s.

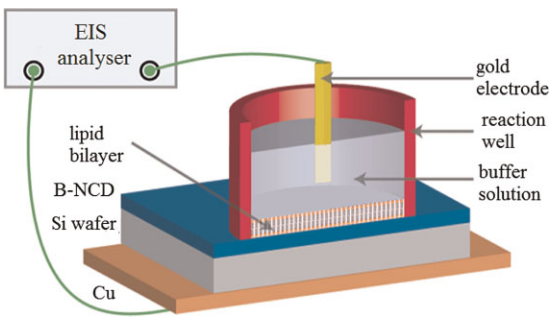


**Figure 1** (online colour at: www.pss-a.com) A schematic cross-section of the setup for EIS measurements. SLB is formed in the measurement well on the B-NCD.

**2.4 Confocal microscopy** Besides EIS experiments we also monitored membrane formation by the means of fluorescent confocal microscopy. In this experiment DOPC:DOPS lipids were marked by 1 μM of fluorescent dye BODIPY D-3795 (Invitrogen, USA) prior to formation of the liposomes. The presence of lipid membrane on B-NCD was investigated by confocal fluorescence microscopy using 488 nm argon-ion laser excitation with maximum intensity at the sample surface of 1.00 mW.

**2.5 Equivalent circuit** To understand the electrical response and changes induced by formation and disruption of the lipid bilayer, the impedance data were analysed using equivalent circuit models with discrete elements. The equivalent circuit that was used for modelling of EIS data provided the most accurate fit for experimental data. This circuit has been used for semiconductors to model processes in sensors in several previous studies [15–17].

As shown in Fig. 2, the equivalent circuit can be divided into three components. (i) The first component represents a series resistance $R_s$, this comprises of the bulk solution and electrode resistance between the gold and the B-NCD working electrode. (ii) The second component is a parallel combination of resistance $R_1$ and a constant phase element $Q_1$ and reflects the combined properties of the lipid bilayer and electrical double layer (here, interpreted to mean any non-uniform distribution of ions near the interface) on the surface of the electrode. (iii) The third component, which corresponds to the space-charge region in the B-NCD, also consists of a parallel combination of a resistance $R_2$ and constant phase element $Q_2$. Data were fitted to the model in EIS Spectrum Analyser (Bondarenko, Russia). The quality of the fit is determined by $\chi^2$, if this is below $1 \times 10^{-3}$ it is a good assumption the used model is the correct one.

The constant phase element has impedance as defined by

$$Z = \frac{1}{Q(i\omega)^n} \tag{1}$$

where $Q$ ($S \cdot s^n$) and the exponent $n$ are adjustable parameters. A value of $n = 1$ is equivalent to the "perfect" capacitor. Values of $n < 1$ are often attributed is the presence of a particular type of surface morphology *e.g.* to surface roughness [18]. Some studies attributed lower values of $n$ to depth depended variation in the charge carrier concentration [19].

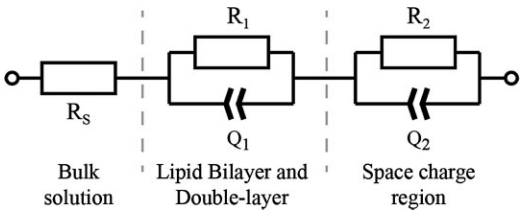


**Figure 2** The equivalent circuit used for modelling divided into components, $R$ represents a resistance; $Q$ is a constant phase element. The individual components of the circuit are explained in the text.

**3 Results and discussion** The data series were fitted over the total measured frequency range from 100 Hz to 1 MHz with $\chi^2$ below $1 \times 10^{-4}$. Resistance of the solution was calculated from eight measurements and was found to be $99\,\Omega \pm 12\,\Omega$.

**3.1 SLB on oxidized B-NCD** Figure 3 shows typical results from oxidized B-NCD. The lipid membrane was measured directly by the EIS during its formation and subsequent melittin-induced disruption. The Nyquist plot in Fig. 3 consists of a semicircle in the higher frequency part of the spectra, which represents the space charge region of diamond; the part of the second semicircle in the lower frequency corresponds to the interface capacitance.

Initially, the impedance was measured when the reaction well was filled only with the buffer solution (squares in Fig. 3). After stabilization of the system, DOPC:DOPS liposomes were added into the reaction well. After 30 min, which is required for the membrane formation, redundant free liposomes in the solution were subsequently flushed with the buffer solution. This step did not result in any significant change of the impedance spectra (circles). The change in the absolute value of the impedance upon formation of the membrane on the electrode surface was small. The absolute value of impedance of the system at frequency of 7.5 kHz, where the impedance is dominated by space charge region, had risen from 1.10 to 1.16 kΩ as obtained by numerical fitting. Introduction of 2 μM of melittin to the reaction well has resulted in a decrease of the absolute of impedance to the value of 1.11 kΩ after 30 min. The impedance semicircle in the spectra had decreased (triangles).

Table 1 summarizes the values of the electrical elements after fitting (using the equivalent circuit shown in Fig. 2). It should be noted that part of the low frequency semicircle is missing as the data contains only frequencies higher than 100 Hz. This leads to a higher uncertainty in the values of the

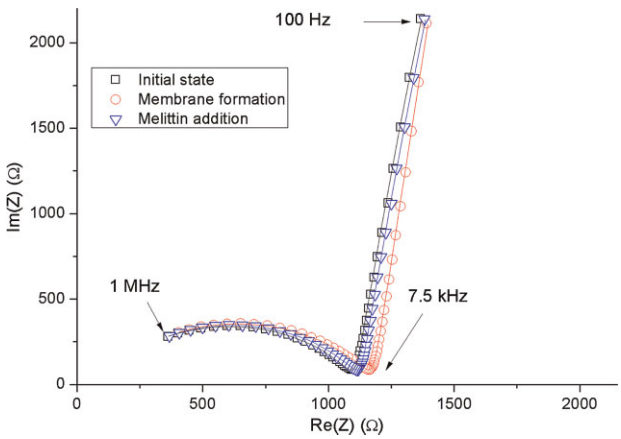


**Figure 3** (online colour at: www.pss-a.com) Nyquist plot showing initial state prior addition of liposomes (□), state after membrane formation (○) and addition of melittin (▽). Fits to the equivalent circuit are indicated with solid lines.

**Table 1** Oxidized B-NCD.

| | initial state | membrane formation | melittin addition |
|---|---|---|---|
| $R_1$ (MΩ) | 1.0 | 1.0 | 1.0 |
| $Q_1$ (μS · s$^n$) | 1.1 | 1.0 | 1.1 |
| $n_1$ | 0.93 | 0.94 | 0.94 |
| $R_2$ (kΩ) | 1.0 | 1.1 | 1.0 |
| $Q_2$ (nS · s$^n$) | 16 | 17 | 16 |
| $n_2$ | 0.75 | 0.74 | 0.75 |

**Table 2** Hydrogenated B-NCD.

| | initial state | membrane formation | melittin addition |
|---|---|---|---|
| $R_1$ (kΩ) | 35 | 223 | 43 |
| $Q_1$ (μS · s$^n$) | 0.49 | 0.75 | 0.54 |
| $n_1$ | 0.94 | 0.86 | 0.95 |
| $R_2$ (kΩ) | 4.46 | 7.40 | 5.62 |
| $Q_2$ (nS · s$^n$) | 0.19 | 0.27 | 0.23 |
| $n_2$ | 0.96 | 0.94 | 0.95 |

elements corresponding of the low frequency semicircle. In general, the values of all elements do not change significantly during membrane formation and subsequent melittin addition. The slightly larger semicircle upon membrane formation results in an increase of $R_2$ from ∼1.0 to ∼1.1 kΩ. The decrease of $R_2$ to ∼1.0 kΩ after addition of melittin corresponds to the change in the smaller semi-circle.

**3.2 SLB on hydrogenated B-NCD** The Nyquist plot in Fig. 4 for the initial state, (i) when only buffer solution was present, (ii) after the membrane formation and (iii) flushing of the redundant free liposomes. A substantial increase in the size of the first semicircle, which corresponds to the molecular bilayer on the B-NCD surface, can be seen. The absolute value of impedance had increased from an initial value of 4.45 to 7.47 kΩ for frequency of 7.5 kHz. The addition of membrane active peptide, melittin, resulted in a decrease in absolute value of impedance to 5.64 kΩ. Data points in the Nyquist plot moved in the direction to the values prior to membrane formation, as the size of the first semicircle decreased.

Values of the electrical elements after fitting data for hydrogenated B-NCD to the equivalent circuit are summarized in Table 2. In contrast to oxidized samples, values of elements of the equivalent circuit change substantially during membrane formation and subsequent melittin addition. The increase in the semicircle upon membrane formation results in an increase of $R_2$ from 4.46 to 7.40 kΩ. From our previous optimization [14], the 200 ppm B is just below the metallic to insulator transitions (concentration of B in these layers is about $6.5 \times 10^{19}$ cm$^{-3}$). In such layers, the resistance is typically >1 MΩ/square which means that one can generate space charge at the interface. Another fact to consider for explanation of the difference in EIS data on H and O-terminated surfaces is the polarization of the water layer on hydrogenated surfaces [20]. In our case, we see a dominant influence of B-NCD behaviour over a wide frequency range for H-terminated surfaces. Value of $R_2$ had decreased to 5.62 kΩ after addition of melittin, indicating membrane disruption.

The difference between initial state and state after the melittin-induced disruption reflects the surface coverage of the membrane residuals on the surface [21].

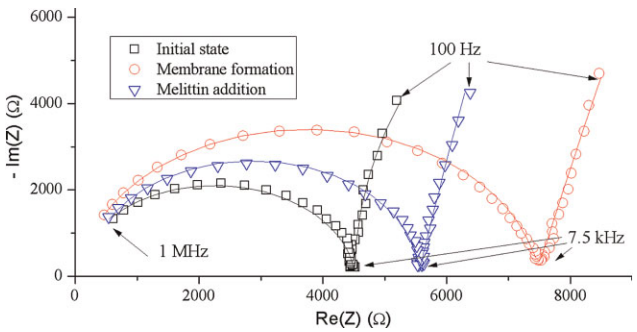


**Figure 4** (online colour at: www.pss-a.com) Nyquist plot representing changes in impedance after addition of liposomes (□), state after membrane formation (○) and addition of melittin (▽). Fits to the equivalent circuit are indicated with solid lines. Change after addition of liposomes into the solution and after membrane disruption is clearly visible.

**3.3 Confocal fluorescent microscopy** To assess the quality of the lipid membrane on oxidized and hydrogenated diamond independently of EIS we took confocal fluorescent microscopy images of liposomes marked by fluorescent dye. Even though the fluorescence signal from hydrogen terminated B-NCD is slightly lower, both surfaces are covered by the lipid membrane. To confirm that the florescence signal originates from phospholipids marked by fluorescent dye, a small area was photobleached by high laser intensity confirming our assumption (see Fig. 5).

**3.4 Comparison of hydrogenated and oxidized surface** Large difference in sensitivity was clearly observed on hydrogenated and oxidized surfaces. H-terminated diamond surface is known for its surface conductivity, induced by transfer doping for undoped diamond films [22]. In this process one transfers an electron from the valence band maximum of diamond ($E_{VBM}$) to the lowest unoccupied molecular orbital (LUMO) level of surface adsorbates. This results in depletion of electrons and consequent pining of the Fermi level ($E_F$) below the $E_{VBM}$ *i.e.* upwards surface band bending, leading to 2D hole gas at diamond surfaces [23]. This effect has been observed for both single crystal and also high quality nanocrystalline diamond films used for construction of FETs [24]. It is obvious that in case of low B doping (200 ppm), reduced below the metallic limits (B concentration $6.5 \times 10^{20}$ cm$^{-3}$),

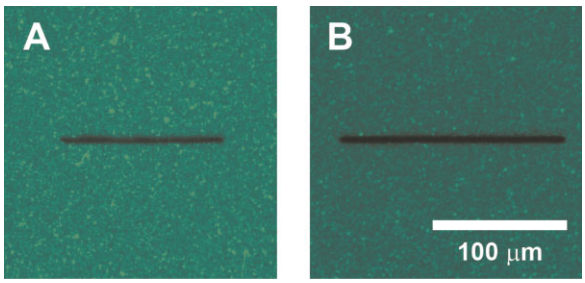


**Figure 5** (online colour at: www.pss-a.com) Confocal fluorescent microscopy images of lipid membranes on (A) oxidized and (B) hydrogenated B-NCD surface. Photobleached area indicating presence of membrane on the surface of the diamond is in the centre of the image.

the $E_F$ lies above the $E_{VBM}$ for O-terminated surface. B-NCD is then semiconducting and surface band bending can develop. However, a difference in boron concentration is present in B-NCD films due to different orientation of the grains 100 and 111. B-uptake adsorbate can play role in surface band bending locally.

While changes in the surface band bending [25, 8] after the lipid membrane formation or disruption would be one of the obvious explanations for the increase in the impedance monitored on H-terminated films, differences in the surface wettability for H and O-terminated surfaces, which was recently discussed in Ref. [20] and which could also contribute to explanation for the observed effects, should also be considered. However, without further focus on the origin of the effect (local changes in the surface bend bending for individual grains with variation of B doping depending on the grain orientation, the surface wettability changes or the changes in band bending profile) our main aim was to evaluate and large changes the EIS data and to model them by equivalent circuit in order to show the difference in doubler layer capacitances for H and O-terminated B-NCD films.

**4 Conclusions** The impedimetric characterization of membrane formation and peptide-induced disruption on hydrogenated and oxidized surfaces of B-NCD was carried out. For hydrogenated surface, significant changes have been observed in the properties of the B-NCD/SLB interface, upon an interaction with the membrane active peptides. The data fitting indicated large changes in the electrical charge kinetics occurring at the diamond surface for H and O-terminated B-NCD/SLB surfaces. While H-terminated surfaces show large changes in impedance after the lipid layer formation or disruption, these changes are negligible for O-terminated B-NCD surface. Several possibilities to explain this observation including changes in the surface band bending profile are discussed.

**Acknowledgements** Financial support from the Academy of Sciences of the Czech Republic (grants KAN200100801 & KAN400480701), the European R&D projects (FP7 ITN Grant No. 238201 – MATCON and COST MP0901 – NanoTP) MSM6840770012 "Transdisciplinary Research in the Field of Biomedical Engineering II." and CTU Grant No. CTU10/811700 are gratefully acknowledged. The Erasmus student exchange programme is also gratefully acknowledged.

## References

[1] K. A. Brogden, Nat. Rev. Microbiol. **3**, 238 (2005).
[2] A. Izadpanah and R. L. Gallo, J. Am. Acad. Dermatol. **52**, 381 (2005).
[3] A. Tossi and L. Sandri, Biopolymers **55**, 4 (2000).
[4] K. Lohner and S. E. Blondelle, Comb. Chem. High Throughput Screen. **8**, 241 (2005).
[5] E. T. Castellana and P. S. Cremer, Surf. Sci. Rep. **61**, 429 (2006).
[6] Y. F. Dufrene and G. U. Lee, Biochim. Biophys. Acta, Biomembr. **20**, 151 (1997).
[7] E. Sackmann, Science **271**, 43 (1996).
[8] P. K. Ang, K. P. Loh, T. Wohland, M. Nesladek, and E. Van Hove, Adv. Funct. Mater. **19**, 109 (2009).
[9] C. E. Nebel, B. Rezek, D. Shin, H. Uetsuka, and N. Yang, J. Phys. D. **40**, 644 (2007).
[10] A. Studer, X. Han, F. K. Winkler, and L. X. Tiefenauer, Colloids Surf. B **73**, 325 (2009).
[11] A. L. Plant, M. Gueguetchkeri, and W. Yap, Biophys. J. **67**, 1126 (1994).
[12] F. Neville, M. Cahuzac, A. Nelson, and D. Gidalevitz, J. Phys.: Condens. Matter. **16**, 2413 (2004).
[13] O. Williams, M. Nesladek, M. Deanen, S. Michaelson, A. Hoffman, E. Osawa, K. Haenen, and R. B. Jackman, Diamond Relat. Mater. **17**, 1080 (2008).
[14] S. D. Janssens, P. Pobedinskas, J. Vacik, V. Petráková, B. Ruttens, J. D'Haen, M. Nesládek, K. Haenen, and P. Wagner, New. J. Phys. **13**, 083008 (2011).
[15] N. Bijnens, V. Vermeeren, M. Daenen, L. Grieten, K. Haenen, S. Wenmackers, O. A. Williams, M. Ameloo,T M. van de Ven, L. Michiels, and P. Wagner, Phys. Status Solidi A **3**, 520 (2009).
[16] W. Yang, M. J. E. Butler, and J. N. Russell, Langmuir **20**, 6778 (2004).
[17] V. Vermeeren, N. Bijnens, S. Wenmackers, M. Daenen, K. Haenen, O. A. Williams, M. Ameloot, M. vandeVen, P. Wagner, and L. Michiels, Langmiuri **23**, 13193 (2007).
[18] M. R. S. Abouzari, F. Berkemeier, G. Schmitz, and D. Wilmer, Solid State Ion. **180**, 922 (2009).
[19] T. Kondo, K. Honda, D. A. Tryk, and A. Fujishima, Electrochim. Acta **48**, 2739 (2003).
[20] M. Dankerl, A. Lippert, S. Birner, E. U. Stützel, M. Stutzmann, and J. A. Garrido, Phys. Rev. Lett. **106**, 196103 (2011).
[21] C. Steinem, H. J. Galla, and A. Janshoff, Phys. Chem. Chem. Phys. **2**, 4580 (2000).
[22] P. Strobel, M. Riedel, J. Ristein, and L. Ley, Nature **430**, 439 (2004).
[23] F. Maier, M. Riedel, B. Mantel, J. Ristein, and L. Ley, Phys. Rev. Lett. **16**, 3472 (2000).
[24] B. Rezek, M. Kratka, A. Kromka, and M. Kalbacova, Biosens. Bioelectron. **26**, 1307 (2010).
[25] A. Hartl, J. A. Garrido, S. Nowy, R. Zimmermann, C. Werner, D. Horinek, R. Netz, and M. Stutzmann, J. Am. Chem . Soc. **129**, 1287 (2007).